Numerical Study on Wave Drift Force of Advancing Ship in Bow Seas

Kyung-Kyu Yang, Yoo-Chul Kim, Kwang-Soo Kim, Jin Kim, Bo Woo Nam, Min-Guk Seo
Korea Research Institute of Ships & Ocean Engineering, Republic of Korea
kkyang@kriso.re.kr

1 Introduction

Wave drift forces and moments are the time averaged forces and moments acting on a floating body in waves. When a ship is advancing in waves, the wave drift force in the longitudinal direction of the ship is called the added resistance in waves. The added resistance in waves is related to the speed loss in actual sea conditions and it is an important issue for reducing greenhouse gas emission to satisfy the energy efficiency design index (EEDI) regulated by International Maritime Organization (IMO). The sway drift forces and yaw drift moments are also important quantities to estimate the ship maneuverability in waves. Recently, many studies regarding the ship maneuvering in waves have been conducted using different methods of computing wave drift forces and moments (Skejic and Faltinsen, 2008; Seo and Kim, 2011; Yasukawa et al., 2019). In this study, wave drift forces and moments acting on an advancing ship in bow waves are investigated using an in-house numerical code that can solve highly nonlinear wave-body interaction problems. The program is called wave and viscous flow analysis system for hull form development (WAVIS) that has been developed by Korea Research Institute of Ships and Ocean engineering (KRISO). Basically, the finite volume method with block-structured mesh and non-staggered allocation is used to discretize unsteady RANS equations. The SIMPLEC method is adapted for velocity pressure coupling and a level-set method is used for free-surface capturing. The overset technique which is implemented in Suggar++ library is adapted for moving body problems. The realizable k-ε model with wall function is applied to model turbulent flows (Kim et al., 2017). Recently, generating oblique waves and solving six degree-of-freedom equations of motion have been implemented to WAVIS code for the present research.

2 Test Case

The target ship in this study is KVLCC2 with Froude number $Fn = U/(gL)^{0.5}$ is equal to 0.142, where U is the ship speed, g is the gravitational acceleration, and L is the ship length. The main particulars of KVLCC2 are summarized in Table 1. In the present numerical method, a non-dimensional form of the governing equation is considered and the Reynolds number for the model scale with 1/100 ratio is used in the following computations. The wave steepness of incident wave is H/L = 0.02 where H means the wave height and the wavelength over the ship length λ/L is varying from 0.5 to 1.5. The incident wave angle β is 150°, which means the incident wave is coming from the bow direction.
To solve the wave-body interaction problems, the overset technique is adapted in this study. The inner domain which is body-fitted structured mesh is moving with the ship motion, whereas the background mesh which has Cartesian grid topology is fixed in time. The background mesh is generated as the incident wave direction and the normal vector at cell faces are aligned. This is one of critical factors to generate the oblique incident waves correctly. The time step is fixed as $T_e/800$ throughout the computations, where T_e means the encounter wave period.

Table 1: Main particulars of KVLCC2.

L	B	D	T	Δ	C_B	Fn
320 m	58 m	30 m	20.8 m	312,622 m^3	0.8098	0.412

3 Results and Discussions

3.1 Convergence tests

To calculate the grid convergence index (GCI; Celik et al., 2008), three different grids were generated – subscript '1' is the finest grid, '3' is coarsest grid, and '2' is in between them and the grid system near the ship surface is shown in Fig. 1, while the background mesh was identical for different inner domain meshes. The total number of grids is varying from 260,000 to 1,410,000 and Table 2 summarizes the ratio of average grid spacing h and the resultant GCI values for the magnitudes of heave, pitch, and yaw motions, added resistance, and yaw drift moment. The ratio of grid spacing is about 1.8, which is larger than that of recommendation value 1.414. The apparent order is about 1.7 which is smaller than 2.0 that is the formal order of accuracy of the present numerical method. The GCIs of motion amplitudes are less than 1.0 %, whereas the added resistance and yaw drift moment are sensitive to the grid spacing. However, the GCIs of added resistance and yaw drift moment lie in the acceptable level compared to the uncertainty of experiment.

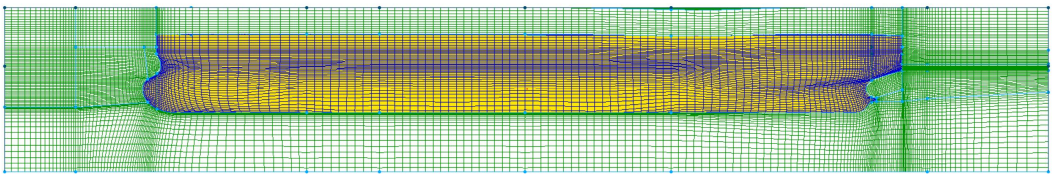

(a) Coarse grid, h_3

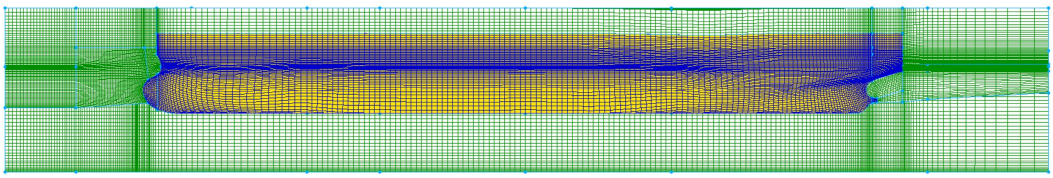

(b) Medium grid, h_2

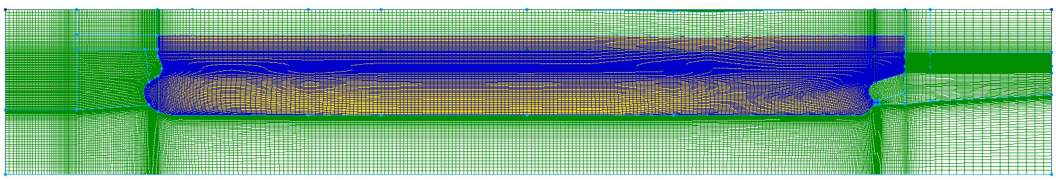

(c) Fine grid, h_1

Fig. 1: Side view of inner domain grids.

Table 2: Grid convergence index of motion responses and drift forces.

	$\lambda/L = 1.1$
h_3 / h_2	1.8486
h_2 / h_1	1.8524
Apparent order	1.753
GCI of heave amplitude (%)	0.782
GCI of pitch amplitude (%)	0.964
GCI of yaw amplitude (%)	0.703
GCI of added resistance (%)	15.33
GCI of yaw drift moment (%)	25.06

3.2 Motion responses and wave drift forces

The snapshots of wave contour and distribution of hydrodynamic pressure on the ship surface are shown in Figs. 2 and 3 for λ/L = 0.5 and 1.1, respectively. The time interval is $T_e/4$ and the hydrodynamic pressure is normalized with linear dynamic pressure ρgA, where ρ is the fluid density and A is the wave amplitude. The wave elevation η is also normalized with the wave amplitude. The black solid line on the ship surface indicates the position at which the level-set function is equal to zero. This iso-surface can be considered as the instantaneous position of free surface.

In the case of short wave (λ/L = 0.5), the ship motion is negligible and thus the ship surface in the weather side is acting like a rigid wall. Consequently, there exist partial standing waves in the weather side, while the incident wave is partially shaded by the ship in the lee side. On the other hand, there exist both diffraction and radiation waves for the resonance condition (λ/L = 1.1). The radiation waves are propagating in both weather and lee sides, while the similar diffraction wave pattern that observed in the short wave case can be seen. However, the amplitude of radiation waves is larger than that of diffraction waves and thus the wave elevation at the ship surface is similar in both weather and lee sides.

The magnitude of six degree-of-freedom ship motions and the wave drift force/moment are summarized in Fig. 4 with respect to the wavelength of incident wave. The diamond symbol represents the result of experiment (Seo et al., 2018) and the rectangular symbol means the result of present numerical method. The added resistance and wave drift force/moment are normalized as follows:

$$Cx = \left(\overline{Fx} - F_0\right) / \left(\rho g A^2 B^2 L\right); \qquad Cy = \overline{Fy} / \left(\rho g A^2 B^2 L\right); \quad Cn = \overline{Mz} / \left(\rho g A^2 B^2\right) \tag{1}$$

where Fx and Fy indicate the hydrodynamic forces in the longitudinal and transverse directions, respectively. Mz means the hydrodynamic moment in the vertical direction and the upper bar indicates the time averaged quantity. F_0 is the total drag in calm water condition, which can be obtained from a separated computation. The figure shows that the present numerical method predicts the motion amplitudes and wave drift force/moment with reasonable accuracy compared to the experimental data. The added resistance shows similar tendency compared to the well-known tendency of added resistance in head waves. In other words, there are mainly two components – diffraction and radiation – of added resistance and only the diffraction wave component exists in short wave region, whereas radiation component also exist as the ship motion becomes large. As the wavelength becomes longer, relative wave elevation along the ship surface becomes zero and thus the added resistance decreases. Further studies with different wave heading angles are required to investigate the effect of heading angles on wave drift force/moment.

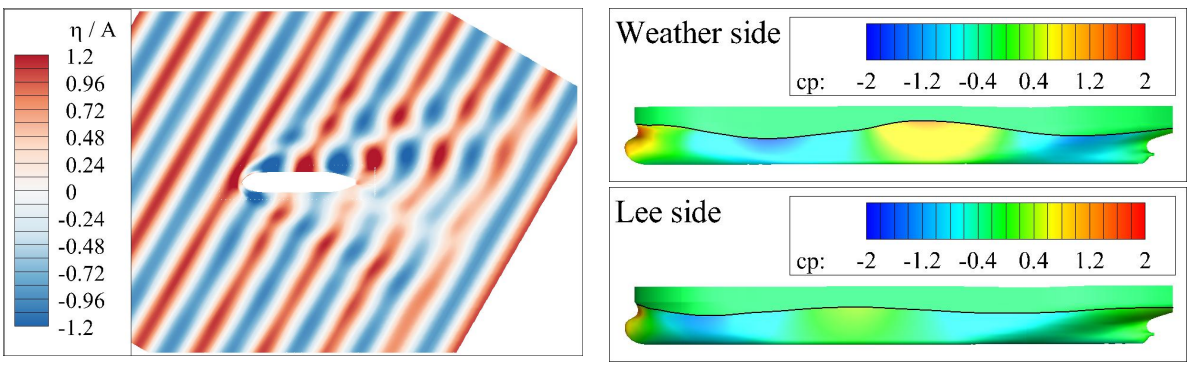

(a) $t = T_0$

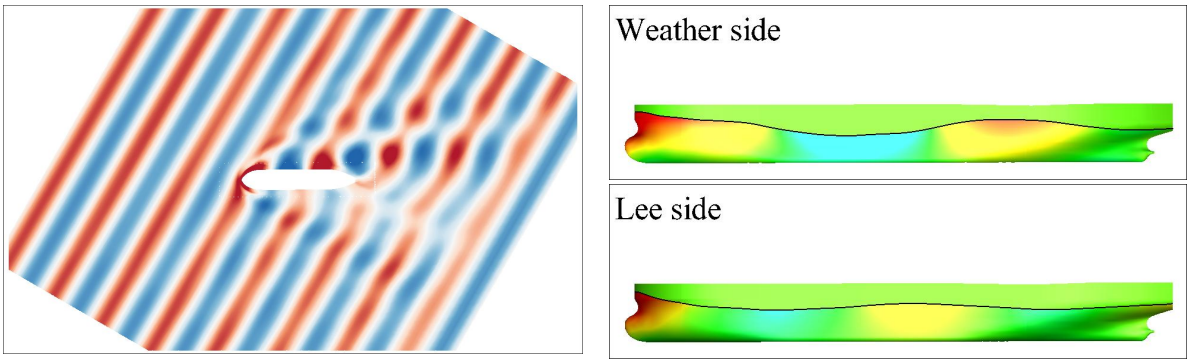

(b) $t = T_0 + T_e / 4$

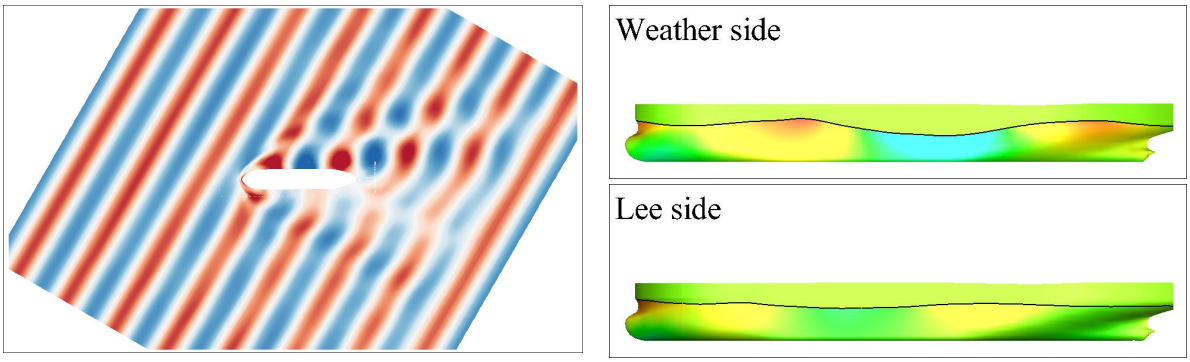

(c) $t = T_0 + 2T_e / 4$

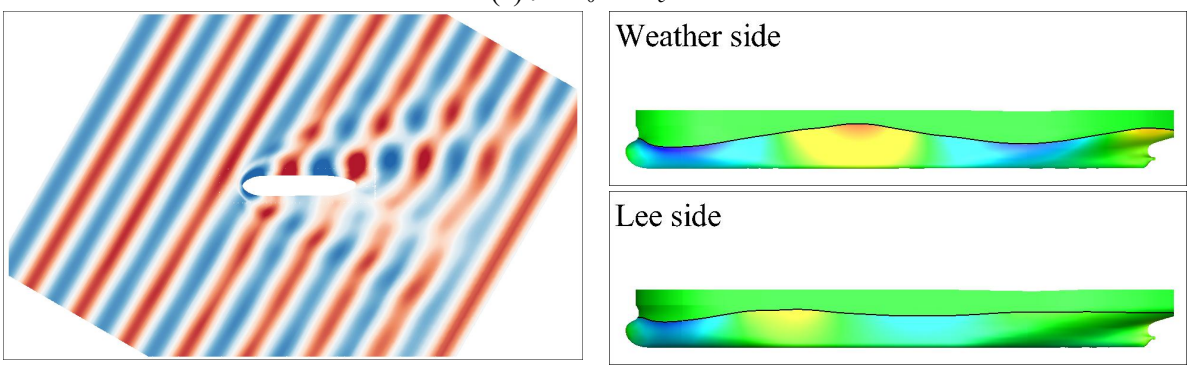

(d) $t = T_0 + 3T_e / 4$

Fig. 2 Snapshots of wave contour (left) and hydrodynamic pressure (right), $\lambda/L = 0.5$, $\beta = 150°$

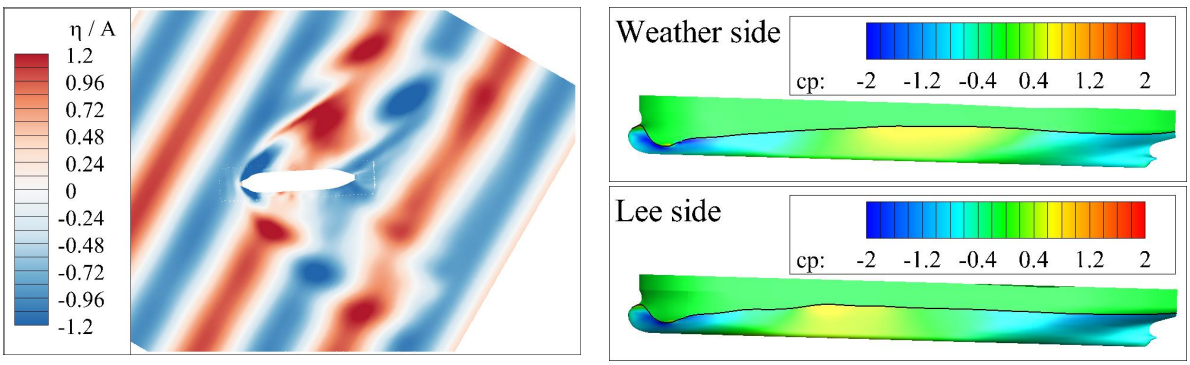

(a) $t = T_0$

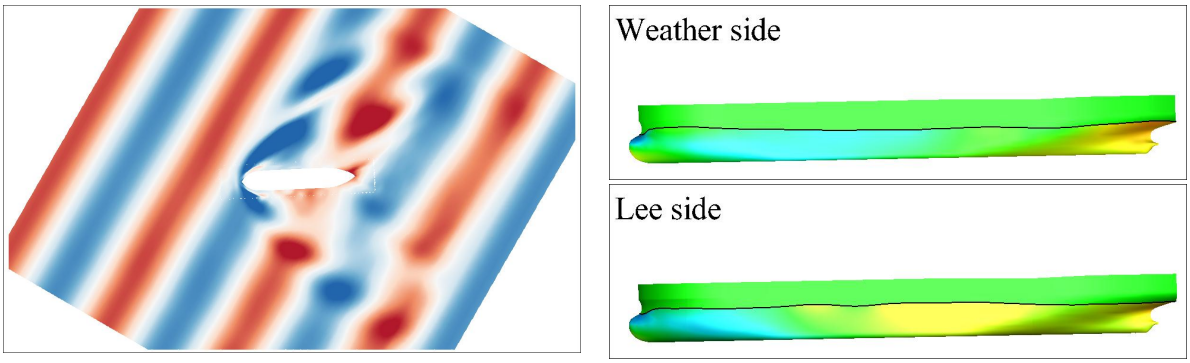

(b) $t = T_0 + T_e / 4$

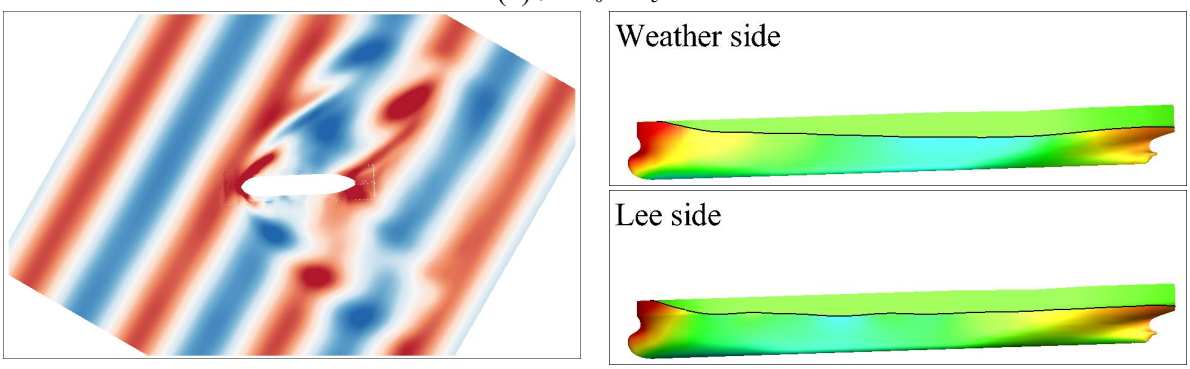

(c) $t = T_0 + 2T_e / 4$

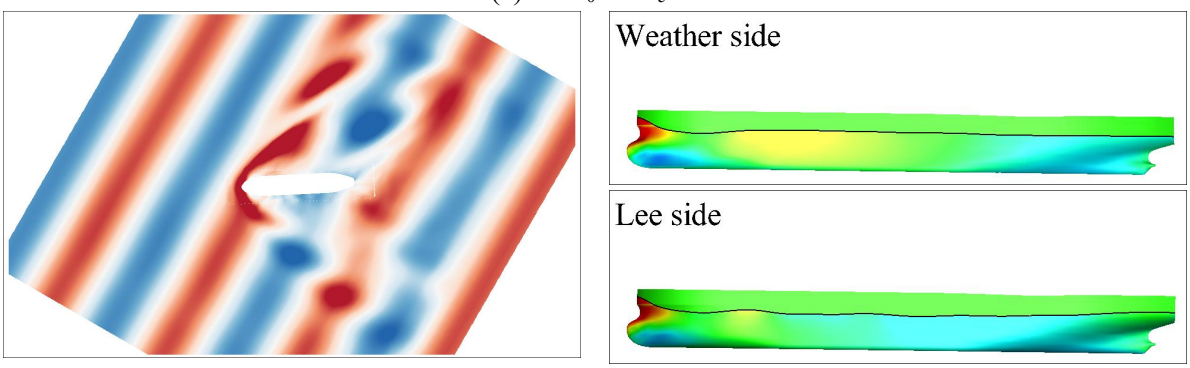

(d) $t = T_0 + 3T_e / 4$

Fig. 3 Snapshots of wave contour (left) and hydrodynamic pressure (right), $\lambda/L = 1.1$, $\beta = 150°$

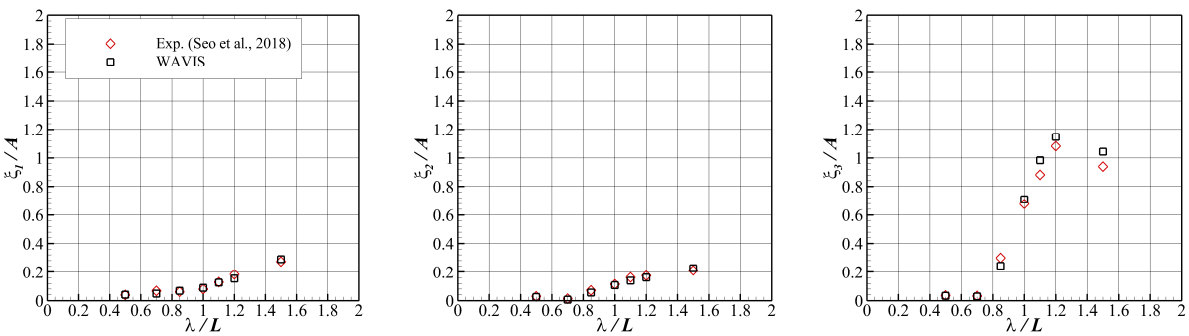

(a) Magnitude of surge motion (b) Magnitude of sway motion (c) Magnitude of heave motion

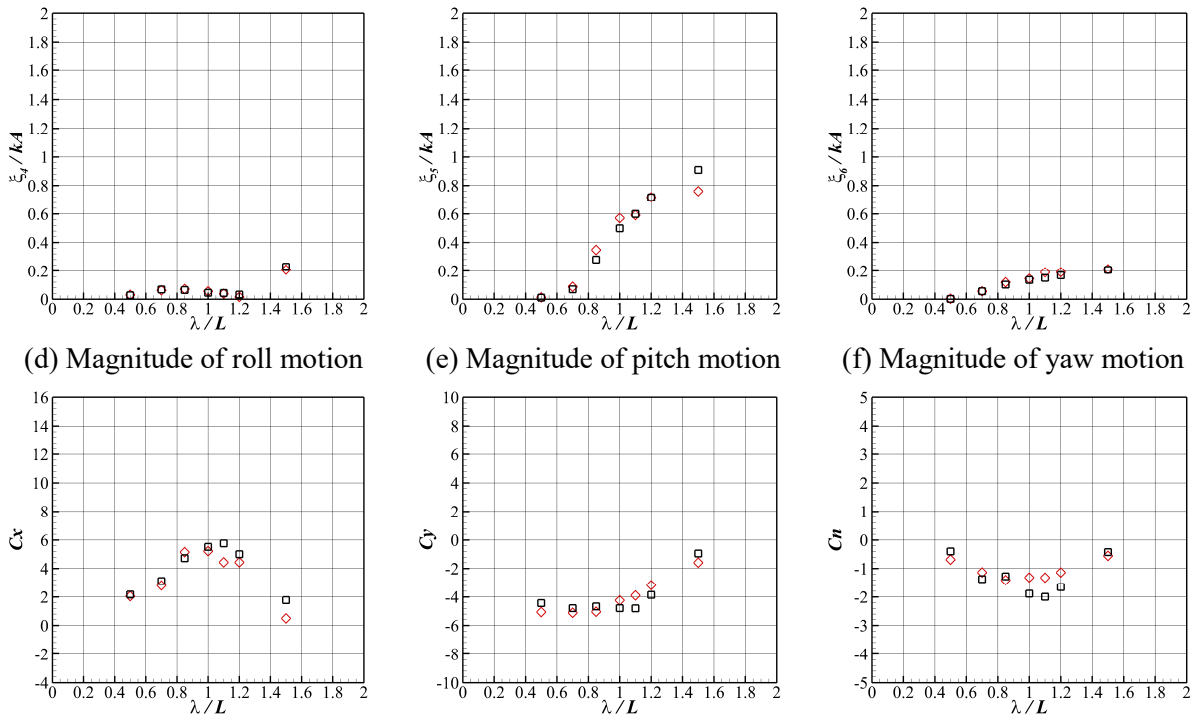

(d) Magnitude of roll motion (e) Magnitude of pitch motion (f) Magnitude of yaw motion

(g) Added resistance (h) Sway drift force (i) Yaw drift moment

Fig. 4 Transfer function of six degree-of-freedom motions and wave drift force/moment, β = 150°

4 Conclusion

In this study, the wave drift forces and moments acting on the ship advancing in bow waves were investigated using the numerical method that is based on the finite volume method with level-set approach and overset grid technique. The present numerical method showed good agreement with the available experimental data of motion responses and wave drift forces and moments. The results for other heading angles will be shown at the Symposium.

Acknowledgements

This research was supported by a grant from Endowment Projects – PES3010 and PES3030 – funded by Korea Research Institute of Ships and Ocean engineering. The authors appreciate all of the support received.

References

R. Skejic and O.M. Faltinsen (2008). A unified seakeeping and maneuvering analysis of ships in regular waves. *J Mar Sci Technol*, **13**(4), 371-394.

M.G. Seo and Y. Kim (2011). Numerical analysis on ship maneuvering coupled with ship motion in waves. *Ocean Eng*, **38**, 1934-1945.

H. Yasukawa, N. Hirata, A. Matsumoto, R. Kuroiwa, and S. Mizokami (2019). Evaluations of wave-induced steady forces and turning motion of a full hull ship in waves. *J Mar Sci Technol*, **24**(1), 1-15.

Y.C. Kim, K.S. Kim, J. Kim, Y. Kim, I.R. Park, and Y.H. Jang (2017). Analysis of added resistance and seakeeping responses in head sea conditions for low-speed full ships using URANS approach. *Int J Nav Archit Ocean Eng*, **9**(6), 641-654.

I.B. Celik, U. Ghia, P.J. Roache, C.J. Freitas, H. Coleman, and P.E. Raad (2008). Procedure for estimation and reporting of uncertainty due to discretization in CFD applications. *J Fluids Eng*, **130**, 078007-078004.

M.G. Seo, B.W. Nam, D.J. Yeo, K. Yun, D.J. Kim, J.Y. Park, and Y. Kim (2018). Numerical analysis of turning performance of KVLCC2 in regular waves. Proceedings of the Annual Autumn Conference, SNAK, Changwon, Korea.